IUBAT Review—A Multidisciplinary Academic Journal, 8(1): 65-84
https://doi.org/10.3329/iubatr.v8i1.83653

Towards Smart Materials: Functional Metallomesogens of Transition Metal Macrocycles and Pyridine Derivative of Long Alkyl Chain

Naima Sharmin[1*], Md. Jahidul Islam[1*], Md. Abu Hanif[1], Md. Hafizul Islam[1], Saiful Islam[1]

[1]*Department of Chemistry, International University of Business Agriculture and Technology (IUBAT), Dhaka, Bangladesh.*

Keywords:

Metallomesogens; Organometallic compound; Copper(II) complexes; Cyclam; 4-Hexadecyloxypyridiene; Magnetic susceptibility

Abstract

Metallomesogenic compounds are an emerging class of materials combining optical, magnetic, and electrical properties, offering great promise for applications in display devices, sensors, and molecular electronics. In this study, a novel copper(II)-based metallomesogen, $[Cu(Cm)(S)_2](J)_2{\cdot}2H_2O$, was synthesized through a four-step synthetic strategy involving cyclam (Cm = 1,4,8,11-tetraazacyclotetradecane), 4-hexadecy-loxypyridine (S), and 4-chlorobenzoate ions (J). Comprehensive characterization was performed using elemental analysis, FTIR, UV-Vis spectroscopy, magnetic susceptibility measurements, TGA, DSC, and polarized optical microscopy (POM). Elemental examination proved the proposed formula, and UV-Vis spectroscopy indicated a trans-III octahedral geometry around the Cu(II) center. The complex exhibited a magnetic moment (μ_{eff}) of 1.7 B.M., typical for mononuclear copper(II) complexes. TGA demonstrated multistep thermal decomposition, while DSC revealed three broad endothermic transitions associated with crystal-to-mesophase, mesophase-to-isotropic, and subsequent cooling transitions. POM analysis further confirmed the formation of mesophases, highlighting the compound's mesogenic behavior. The successful synthesis and detailed study of $[Cu(Cm)(S)_2](J)_2{\cdot}2H_2O$ provide important insights into the design of new metallomesogens with tunable physical properties, expanding opportunities for future development in advanced materials for electronic and optoelectronic applications.

Cm = (1,4,8,11-tetraazacyclotetradecane),
S = 4-hexadecy-loxypyridine, and
J = 4-chlorobenzoate ions (J)

[*]Corresponding authors' E-mail address: jahidul.che@iubat.edu
Article received: March 2025 Revised and accepted: June 2025 Published: June 2025

Graphical abstract

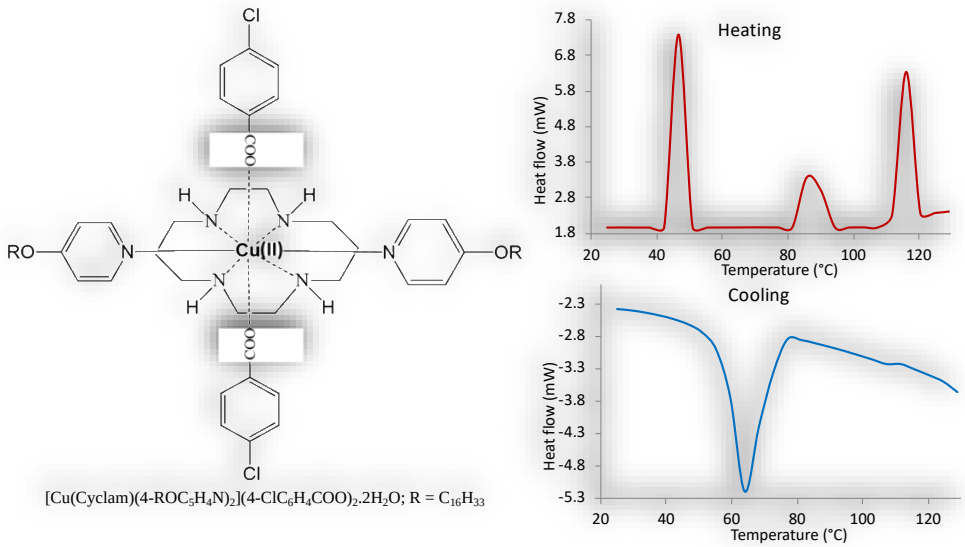

1. Introduction

One unique state of matter that contains properties halfway between those of liquids and solids is liquid crystals (Andrienko, 2018). They possess the fluidity of liquids but also possess a degree of molecular order, similar to solids (Santos, Figueirinhas, Dionísio, Godinho & Branco, 2024). This molecular arrangement allows them to respond to external stimuli like temperature, electric fields, and light, leading to a variety of optical and electronic properties (Li & Li, 2020; Li & Yin, 2019). Liquid crystals are widely used in displays, such as those found in televisions, computer monitors, and smartphones, as well as in optical devices like lenses and shutters (Aljamali & Molim, 2021; Yin *et al.*, 2022) Metallomesogens are unique substances that combine the properties of metal complexes and liquid crystals. These materials exhibit liquid-crystalline phases, similar to purely organic liquid crystals, due to the interactions between their anisotropic molecules (Cuerva, Cano, & Lodeiro, 2021). While mononuclear complexes have dominated metallomesogen research, introducing additional metal centers into these structures holds the potential for exciting new properties (Cook & Stang, 2015). For instance, binuclear carboxylates of divalent metal ions of transition series, such as copper(II), rhodium(II), ruthenium(II), molybdenum(II), palladium(II), and chromium(II), have been extensively studied and offer a promising avenue for exploring novel magnetic and electronic behaviors (Islam *et al.*, 2024; Yufanyi, Abbo, Titinchi, & Neville, 2020)

The metal-free macrocycles exhibited columnar liquid crystal phases at room temperature, with the phase transition temperature varying depending on the chain length (Ghosh, 2024). Introducing metal ions into these macrocycles is

expected to maintain the columnar arrangement, leading to the formation of similar columnar phases in the corresponding metal complexes (Kawano, Murai, Harada, & Tanaka, 2018). This prediction is based on the structural similarity between the metal-free and metal-containing macrocycles, suggesting that the metal ions do not significantly disrupt the overall molecular packing and arrangement (Islam & Islam, 2025a; Koifman *et al.*, 2020). When disk-like mesogens are arranged in columns; it gives rise to a suitable building block for anisotropic materials for exploiting those in electronic industries to manufacture conductors that are one dimensional, photoconductors, molecular fibers and wires, LEDs and photovoltaic (PV) cells (Chakrabarty *et al.*, 2023; F. Guo & Hurt, 2017). A variety of transition metals, such as Pt, Pb, Cr, Mo, W, Lu, Co, Ni, Pd, Cu, and Zn, have been incorporated with several macrocyclic tridentate, tetradentate hexadentate and octadentate ligands to achieve hexagonal or rectangular columnar arrangements of discotic molecules (Chakrabarty, Mim, Tonu, Ara, & Dhar, 2024; Islam, Ara, Naime, & Khan, 2024; Nasiri Sovari & Zobi, 2020; Thakur *et al*., 2022). It is evident that the mesophases of the macrocyclic metallomesogens are more stable than that of their open chain counterpart (Islam *et al*., 2025; Marti-Centelles, Pandey, Burguete, & Luis, 2015). In addition to stable mesophase; their self-assembly properties draw the researchers' attention for manufacturing commercial electronics especially (C. Li et al., 2020). However, there are not a significant number of examples of metallomesogens where metals are fused in 1,4,8,11-tetraazacyclotetradecane (cyclam); reported in the literature (Sharmin *et al*., 2025).

Metallomesogens, while offering unique properties, face limitations and challenges in their synthesis and applications (Xu, Li, Yin, & Huang, 2024). The incorporation of metal ions into liquid crystal structures can introduce complexities in the synthesis process, such as controlling the coordination environment of the metal and ensuring the formation of stable mesophases (Cho & Ishida, 2017). Additionally, the selection of metal ligands and ions significantly influences the properties of the resulting metallomesogens, making it challenging to design materials with specific properties (Islam & Islam, 2025b; Xu *et al*., 2024). Furthermore, the potential applications of metallomesogens are often limited by their thermal stability, solubility, and processibility. These factors can hinder their integration into practical devices and materials (Wang, Astruc, & Abd-El-Aziz, 2019). Overcoming these limitations requires a deeper understanding of the fundamental principles governing the formation and behavior of metallomesogens, as well as the development of innovative synthetic strategies and processing techniques.

Despite the promising potential of metallomesogens, there remains significant room for optimization and calibration to achieve their full potential in practical applications. This research aims to contribute to this field by focusing on the synthesis, thermochemical properties evaluation, and structural analysis of metallomesogens based on Cu(II) complexes with the cyclam ligand. By comprehensively studying these aspects, we aim to gain valuable insights into the

factors influencing the properties and performance of these materials, paving the way for future advancements and applications.

In this work, the successful synthesis and detailed characterization of a new copper(II)-based metallomesogen coordinated with cyclam and 4-hexadecyloxypyridine ligands addresses an important gap in the field of metallomesogens, particularly those incorporating macrocyclic ligands like cyclam. The complex $Cu(Cm)(S)_2(J)_2 \cdot 2H_2O$ exhibits unique mesomorphic and magnetic properties, combining thermal stability, ionic liquid behavior, and octahedral coordination geometry. Such a synergistic combination of structural, magnetic, and mesophase properties broadens the scope of functional metallomesogens and lays the groundwork for their future application in electronic, optoelectronic, and smart material technologies. This research not only enriches the limited library of cyclam-based metallomesogens but also provides a strategic pathway for designing tunable advanced materials.

2. Materials and Methods

This study target to examine the synthesis and characterization of magnetic metallomesogen,$[Cu(Cm)(H_2O)_2](J)_2.2H_2O$ Where Ligand (S) – 4- Hexadecyl pyridiene ($4\text{-}CH_3(CH_2)_{15}OC_5H_4N$); Cyclam (Cm) - 1,4,8,11-Tetraazacyclotetradecane; J - $4\text{-}ClC_6H_4COO^-$**.** The metallomesogen incorporates a Cu(II) ion coordinated with cyclam, a macrocyclic ligand, and a functionalized benzoate derivative with fluorine at position 4. The synthesis involved a multi-step process starting with 4-iodo benzoate, 1-bromohexadecane, and cyclam as precursors. By carefully selecting solvents and reaction conditions, we successfully obtained the target metallomesogen. Subsequent characterization studies aimed to elucidate the structural, magnetic, and liquid crystal properties of this compound using FTIR, NMR, UV, TGA, DSC and polarized optical micrograph (POM).

2.1. Experimental: Materials

Sigma-Aldrich and Merck supplied the following reagents, which have been used without any further processing.: 4-hydroxypyridine (C_5H_5NO, 95%), 4-chlorobenzoate ($C_7H_4ClO_2K$, 99%), 1-bromohexadecane ($CH_3(CH_2)_{15}Br$, 98%), potassium carbonate (K_2CO_3, 99.995%), potassium iodide (KI, 99.0%), potassium hydroxide (KOH, 99.995%), ethanol (C_2H_5OH, 99.55%), dimethylformamide (99.8%), copper sulfate pentahydrate ($CuSO_4 \cdot 5H_2O$, 98.0%), and cyclam ($C_{10}H_{24}N_4$, 1,4,8,11-Tetraazacyclotetradecane, 98%). Figure 1 presents the raw materials used in this research.

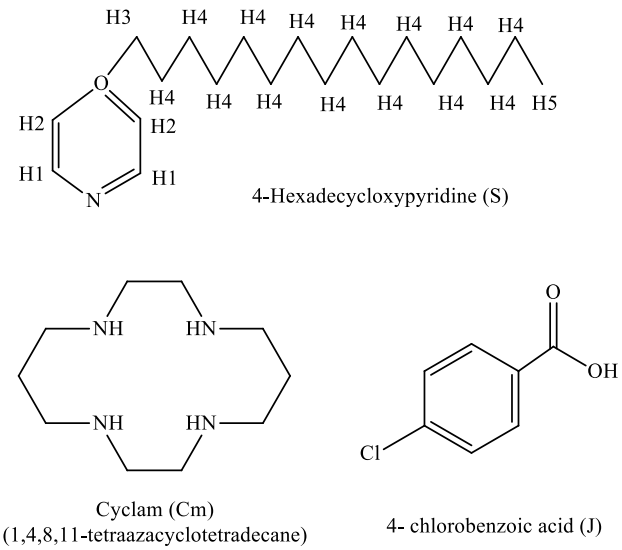

Figure 1: Chemical formula of the corresponding ligand used for synthesis of copper metal associated liquid crystal $[Cu(Cm)(S)_2](J)_2.2H_2O$; Where Ligand (S) – 4- Hexadecyl pyridine ($4\text{-}CH_3(CH_2)_{15}OC_5H_4N$); Cyclam (Cm) - 1,4,8,11-Tetraazacyclotetradecane; J - $4\text{-}ClC_6H_4COO^-$.

2.2. Experimental: Methods of Synthesis

For synthesizing liquid crystal $[Cu(Cm)(S)_2](J)_2.2H_2O$; Where Ligand (S) – 4-Hexadecyloxy pyridine ($4\text{-}CH_3(CH_2)_{15}OC_5H_4N$); Cyclam (Cm) - 1,4,8,11-Tetraazacyclotetradecane; J - $4\text{-}ClC_6H_4COO^-$; the process started with the 4-(hexadecyloxy) pyridine ligand synthesis. The synthesis of this 4-(hexadecyloxy) pyridine involved a nucleophilic substitution reaction between 1-bromotetradecane and 4-hydroxypyridine. Potassium carbonate (K_2CO_3) and potassium iodide (KI) were used as a base and catalyst, respectively. The reaction was carried out in dimethylformamide (DMF) at reflux for 24 hours. The product was collected after filtering. Further rinsing and recrystallization using ethanol was done. After dehydrating the yield was 88.8%. The multistep synthesis process of $Cu(Cm)(S)_2](J)_2.2H_2O$ including the corresponding intermediate ligand and complexes are illustrated in the Figure 2.

In the second step of the metallomesogen synthesis of $Cu(Cm)(H_2O)_2](J)_2.2H_2O$, dinuclear copper(II) complexes with the formula $[Cu_2(J)_4(EtOH)_2].2H_2O$, were synthesized through a solution-based reaction. Copper sulphate pentahydrate ($CuSO_4.5H_2O$) and potassium 4-chlorobenzoate ($4\text{-}ClC_6H_4COOK$) were combined in ethanol (EtOH) and heated for 30 minutes. This reaction resulted in the formation of the desired dinuclearcopper(II) complexes, likely involving the coordination of the 4-chlorobenzoate ligands to the copper ions and the inclusion of ethanol and moisture.

The third step was associated with the synthesis of $[Cu(Cm)(H_2O)_2](J)_2.2H_2O$ (copper(II) complex). A warmed ethanolic suspension of the copper precursor was mixed with an ethanolic solution of cyclam, $[Cu_2(J)_4(EtOH)_2].2H_2O$. After that, the purple mixture was boiled and filtered, yielding the desired complex as needle like crystals having purple color with a product of 64.8%.

In the fourth and final step of the synthesis of $[Cu(Cm)(S)_2](J)_2.2H_2O$ liquid crystal, $[Cu(Cm)(H_2O)_2](J)_2.2H_2O$ complex and ligand (S) which was 4-Hexadecyloxy pyridine was dissolved in ethanol and heated to facilitate the reaction. The resulting product, $[Cu(Cm)(S)_2](J)_2.2H_2O$, was gained as a amorphous powder of dark purple color after filtration and cooling. Yield of the reaction was 66.7%, indicating a reasonable conversion of the starting materials to the desired product.

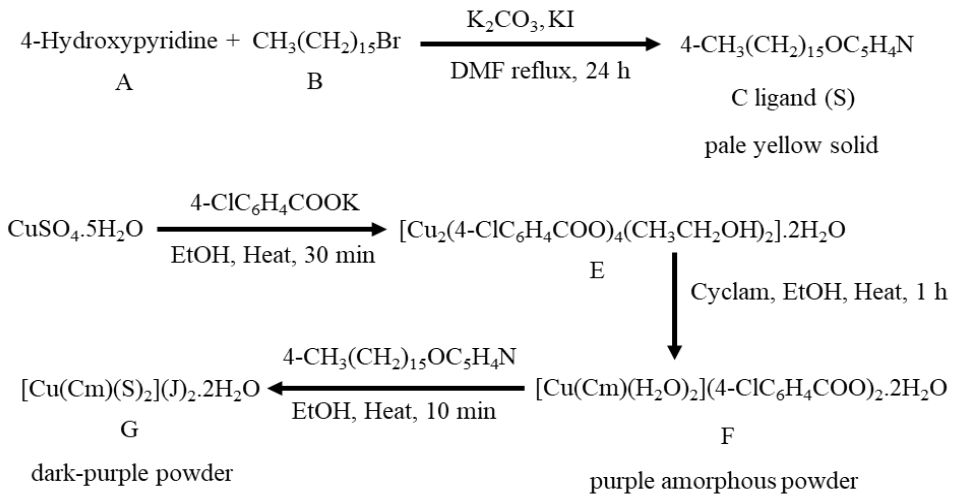

Figure 2: Synthesis scheme of $[Cu(Cm)(S)_2](J)_2.2H_2O$ liquid crystal; where Ligand (S) – 4-Hexadecyloxy pyridine ($4\text{-}CH_3(CH_2)_{15}OC_5H_4N$); Cyclam (Cm) - 1,4,8,11 Tetraazacyclotetradecane; J - $4\text{-}ClC_6H_4COO^-$.

2.3. Experimental: Instrumental Investigation

2.3.1. Elemental Investigation

A Perkin-Elmer CHNS/O 2400 Series II elemental analyzer had been employed to conduct elemental analysis on the samples. Each test samples were accurately weighed on an AD-6 microbalance. The samples were then encapsulated in small aluminum capsules (5 x 8 mm) and tightly folded to ensure a secure fit within the analyzer column. Subsequently, the encapsulated samples were introduced into analyzer and subjected to high temperatures, reaching a highest of 1000 °C, to facilitate the complete combustion and analysis of the elemental composition.

2.3.2. ^{1}H-Nuclear magnetic resonance spectroscopy

A 400 MHz frequency spectrometer manufactured by the JEOL firm was used for collecting the sample's proton nuclear magnetic resonance (^{1}H-NMR) spectrum. A small quantity of the compound was made to dissolve in deuterated chloroform ($CDCl_3$) to serve as the solvent. $CDCl_3$ is a common solvent choice for NMR spectroscopy due to its deuterium nuclei, which do not interfere with the detection of proton signals.

2.3.3. Fourier transform infrared spectroscopy

The FTIR spectra of the samples were collected using a Perkin-Elmer Spectrum 400 FT-IR/FTR/Pike 22107 Technologies Cladi ATARTM spectrometer in the spectral range of 4000-400 cm^{-1}. A little quantity of neat analyte was put in diamond anvil cell, ensuring direct contact between the detector and the sample surface. This configuration facilitated accurate measurement and analysis of the vibrational spectra.

2.3.4. Magnetic susceptibility

The magnetic properties of the synthesized complexes were investigated using the Gouy method to determine their gram magnetic susceptibility (χg) at 298 K, room temperature. A Sherwood Auto machine was employed to measure Magnetic susceptibility, with distilled water serving as the calibrant. That finely ground samples were put into a cylindrical shape tube having length of approximately 1.5 cm, as well their weight was recorded. The tube was then placed in the instrument to measure the χ_g value. The diamagnetic contribution (χ_{dia}) of each atom in the molecule was calculated using Pascal's constants allowing for the determination of the molar susceptibility (χ_m). By subtracting the diamagnetic contribution from the molar susceptibility, the corrected molar susceptibility (χMcorr) was obtained. Finally, the value of magnetic moment was obtained by exploiting the equation, $\mu_{eff} = 2.828(\chi M_{corr} T)^{½}$, where T is the temperature in Kelvin.

2.3.5. UV-visible spectroscopy

The absorbance of the sample was measured using a UV-visible-NIR spectrophotometer across a wavelength range of 300 to 2000 nm. The sample was prepared by dissolving it in a suitable solvent and transferring the solution to a cuvette made of quartz. The spectrum was tallied relative to the used solvent, ensuring that any absorbance observed was due to the sample itself. This technique allows for the identification and quantification of specific chemical species based on their characteristic absorption patterns within the specified wavelength range.

2.3.6. Polarizing optical microscopy

Applying an Olympus polarizing optical microscope outfitted with a Linkam THMS 600 hot stage and a central processor of FP90 model from Mettler Toledo, photomicrographs of the synthesized complexes were captured. Prior to analysis, the samples were nicely ground as well dried by oven setting temperature at 60 °C

for overnight to remove any residual moisture. Heating/cooling scale were systematically changed within 2 - 10 °C/min to investigate their influence on the observed phenomena. The magnification used for imaging was 50x, providing a detailed view of the sample morphology and any temperature-dependent changes.

2.3.7. Thermogravimetry

The Perkin-Elmer 4000 TG/DTA Thermal System was used to perform thermogravimetric analysis (TGA)**.** Under a nitrogen environment (10 cm^3/min), samples (2–5 mg) were heated in a ceramic pan from 35°C to 900°C at a rate of 20°C/min. Weight loss was tracked in relation to temperature in the analysis, providing information about the thermal stability and decomposition behavior of the samples.

2.3.8. Differential scanning calorimetry (DSC)

DSC was conducted using both a Perkin-Elmer DSC6 and METTLER TOLEDO DSC822 and a to analyze the thermal properties of the sample. After precisely weighing 2–8 mg of the sample, it was put in an aluminum crucible. After that, the crucible was placed into the DSC heating stage and heated and cooled several times between 25 and 300 °C at a scan rate of 10 °C per minute. To reduce oxidation and other environmental influences that can have an impact on the results, the analysis was carried out in a nitrogen atmosphere at a flow rate of 10 cm^3/min.

3. Results and Discussion

The target of this investigation was to synthesize and evaluate magnetic and metallomesogens properties of a compound with the formula $[Cu(Cm)(S)_2](J)_2.2H_2O$. The ligand S, 4-hexadecyloxy pyridine, is a long-chain alkyloxy pyridine derivative, while Cyclam (Cm) is a macrocyclic tetraamine ligand. The counterion J is 4-chlorobenzoate. The synthesized compounds were then evaluated for their liquid crystal properties. This investigation aimed to explore the potential of these metallomesogens as functional materials with unique magnetic and liquid crystalline characteristics.

3.1. Synthesis and Characterization of Hexadecyloxypyridine-4 Ligand (S)

4-Hexadecyloxypyridine (S) was successfully synthesized through a nucleophilic substitution reaction between hydroxypyridine-4 and bromohexadecane-1 in presence of a base (K_2CO_3) and a catalyst (KI) in dimethylformamide (DMF). The reaction yielded a pale brown powder with an 88.8% yield, indicating good efficiency.

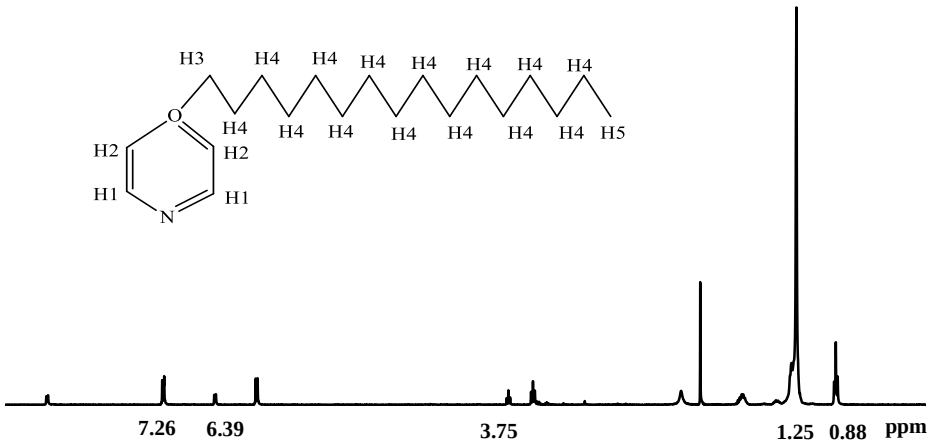

Figure 3: ^{1}H NMR of 4-hexadecyloxypyridine taken in $CDCl_3$ in 400 MHz frequency machine.

The structure of S was confirmed by ^{1}H-NMR spectroscopy. The aromatic protons exhibited a multiplet at 7.26, as well as a quartet at 6.39 in ppm, respectively (Forensi, Stopin, de Leo, Wouters, & Bonifazi, 2020). The methylene protons adjacent to the oxygen atom appeared as a triplet peak at 3.75 in ppm (Rosenthal, Puskas, & Wesdemiotis, 2012). The remaining -CH_2- protons within the alkyl chain resonated as a multiplet at 1.25 ppm. Finally, the terminal methyl protons were observed as a triplet at 0.88 ppm (Kluenker, Mondeshki, Nawaz Tahir, & Tremel, 2018). ^{1}H NMR of 4-hexadecyloxypyridine which is taken in $CDCl_3$ in 400 MHz frequency machine were shown in the Figure 3.

Elemental analysis of the ligand (S = 4- Hexadecyl pyridine (4-$CH_3(CH_2)_{15}OC_5H_4N$) confirmed its chemical formula as $C_{21}H_{37}NO$. Molecular weigh 319.5. The calculated and found elemental percentages closely matched Calc.: H: 11.67; C: 78.94; N: 14.07%. Found: H: 12.10; C: 79.01; N: 13.88%)., further supporting the proposed formula. Elemental analysis results of [Cu(Cm)(4-$CH_3(CH_2)_{15}OC_5H_4N)_2$](4-$ClC_6H_4COO)_2.2H_2O$ compounds and its precursors and intermediates were shown in the Table 1.

Table 1: Elemental examination outcomes of $[Cu(Cm)(S)_2](J)_2.2H_2O$ and its precursor and ligand.

Compound notations	Molecular Formula	Formula Weight (g/mol)	Examination outcomes	yield%
$4\text{-}CH_3(CH_2)_{15}OC_5H_4N$	$C_{21}H_{37}NO$	319.52	Calc.: C, 78.9; H, 11.6; N, 14.07% Found: C, 79.1; H, 12.1; N, 13.8%	88.8
$[Cu(Cm)(H_2O)_2](J)_2.2H_2O$	$C_{24}H_{40}CuCl_2N_4O8$	647.1	Calc.: C, 44.5; H, 6.2; N, 8.7% Found: C, 44.1; H, 6.1; N, 8.8%	64.8
$[Cu(Cm)(S)_2](J)_2.2H_2O$	$C_{66}H_{110}CuCl_2N_6O_8$	1250.1	Calc.: C, 63.4; H, 8.9; N, 6.7% Found: C, 63.1; H, 8.5; N, 6.7%	66.7

The FTIR analysis of the ligand (S) of 4-hexadecyloxypyridine ($4\text{-}CH_3(CH_2)_{15}OC_5H_4N$) exhibited characteristic peaks indicative of the occurrence of common functional groups. Two prominent bands at 2851 cm^{-1} and 2919 cm^{-1} corresponded to the symmetric and asymmetric stretching vibrations of the methylene (CH_2) group, respectively (Wang, Dan, Zhang, Ma, & Lin, 2023). A medium-intensity band at 1638 cm^{-1} confirmed the presence of the C=N stretching vibration associated with the pyridine moiety (Karpagakalyaani, Magdaline, & Chithambarathanu, 2022). Additionally, a medium band at 1287 cm^{-1} was attributed to the stretching vibration of C-N of the pyridine ring, while a strong band at the value of 1188 cm^{-1} indicated the stretching vibration of C-O to the ether portion (Yusuf, 2023). These spectrum findings aligned with the compound's predicted structure, as depicted in the Figure 4.

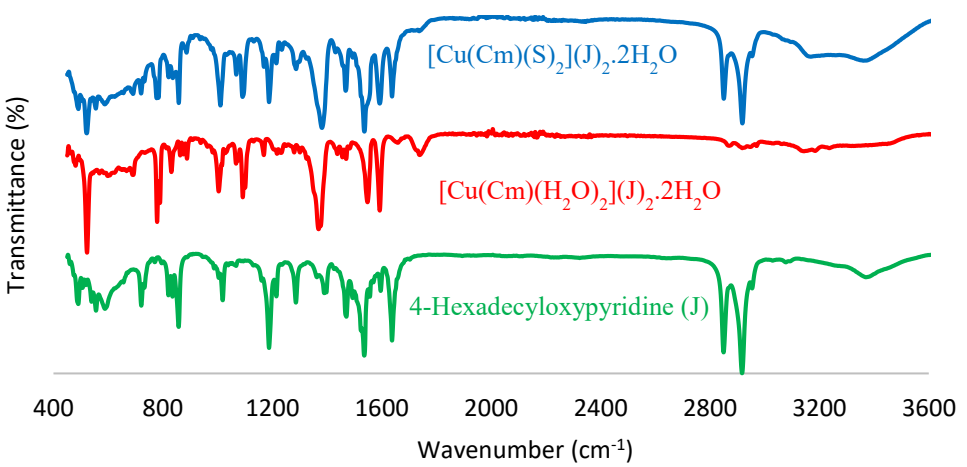

Figure 4: Data assignments by FTIR of Ligand (L), $[Cu(Cm)(H_2O)_2](J)_2.2H_2O$ and $[Cu(Cm)(S)_2](J)_2.2H_2O$; Where Ligand (S)– 4- Hexadecyloxy pyridine ($4\text{-}CH_3(CH_2)_{15}OC_5H_4N$); Cyclam (Cm) - 1,4,8,11-Tetraazacyclotetradecane; J - $4\text{-}ClC_6H_4COO^-$

Table 2: Data assignments by FTIR of Ligand (S), $[Cu(Cm)(H_2O)_2](J)_2.2H_2O$ and $[Cu(Cm)(S)_2](J)_2.2H_2O$; Where Ligand (S) – 4- Hexadecyloxy pyridine (4-$CH_3(CH_2)_{15}OC_5H_4N$); Cyclam (Cm) - 1,4,8,11-Tetraazacyclotetradecane; J - 4-$ClC_6H_4COO^-$

Complex	Wavenumber (cm^{-1})					
	O-H	N-H	CH_2	COO	C-O	C-N
4-Hexadecyloxypyridine (J)	-	-	2919 (asym) 2851s (sym)	1538s	1188s	1287s
$[Cu(Cm)(H_2O)_2](J)_2.2H_2O$	3342br	3200br	-	1548m (asym) 1374s (sym)	-	1095m
$[Cu(Cm)(S)_2](J)_2.2H_2O$	3359br	3183br	2915s (asym) 2849s (sym)	1638m (asym) 1472s (sym)	1284s	1189m

3.2. Synthesis and Chemical Structural Elucidation of $[Cu(Cm)(H_2O)_2](J)_2.2H_2O$

The coordination complex $[Cu(Cm)(H_2O)_2](J)_2.2H_2O$ was synthesized through a two-step process**.** Initially, the copper(II) complex $[Cu_2(J)_4(EtOH)_2].2H_2O$ was prepared by a solution-based method. Copper sulfate pentahydrate and potassium 4-chlorobenzoate were dissolved in ethanol and heated for 30 minutes, resulting in the formation of the desired complex.

In the second step of complex synthesis, $[Cu_2(J)_4(EtOH)_2].2H_2O$ was reacted with cyclam in ethanol to form a copper-cyclam intermediate. Later, the ligand S was introduced to this intermediate, resulting in the formation of the compound $[Cu(Cm)(H_2O)_2](J)_2.2H_2O$. The product yielded 64.8% and has been separated as purple powder. Elemental investigation of the complex affirmed its chemical formula as $C_{24}H_{40}CuCl_2N_4O_8$, indicating the presence of copper (Cu), cyclam (a macrocyclic ligand), 4-chlorobenzoate anions, and water molecules of hydration. The calculated and found elemental percentages closely matched Calc.: C, 44.5; H, 6.2; N, 8.7%, Obtained: C, 44.1; H, 6.1; N, 8.8%.

The FTIR analysis of $[Cu(Cm)(H_2O)_2](J)_2.2H_2O$ displayed a broad band at 3375 cm^{-1} due to O-H stretching of water molecules, and another broad band at 3189 cm^{-1} attributed to N-H stretching of the secondary amine group (Chukwu & Lohdip, 2024). Additional bands were observed at 1378 cm^{-1} (strong intensity) and 1592 cm^{-1} (medium intensity), corresponding to the symmetric ($\nu_{sym}COO$) and asymmetric ($\nu_{asym}COO$) stretching modes of the carboxylate group, respectively (Liu *et al*., 2020). Furthermore, a medium band at 1096 cm^{-1} was indicative of C-N stretching. The calculated ΔCOO value of 166 cm^{-1} is consistent with the presence of non-coordinated 4-$ClC_6H_4COO^-$ ions (Sheldrick, 2008), as confirmed by the molecular structure. The FTIR results are shown in the Figure 4. Other peaks were shown in Table 2

The UV-vis data of the complex $[Cu(Cm)(H_2O)_2](J)_2.2H_2O$ in $CHCl_3$ displayed a wide d-d band at 544 nm (ε_{max} = 75.7 $(M.cm)^{-1}$, indicating a trans-III octahedral geometry. This observation matches existing literatures on comparable complexes (Brandenburg & Putz, 2006; Macrae *et al*., 2006). The agreement between the solid-state molecular structure and the solution-phase UV-vis spectrum suggests that the octahedral geometry is retained in both environments (Dwivedi, Sunkari, Verma, & Saha, 2018).The UV results are shown in the Figure 5a.

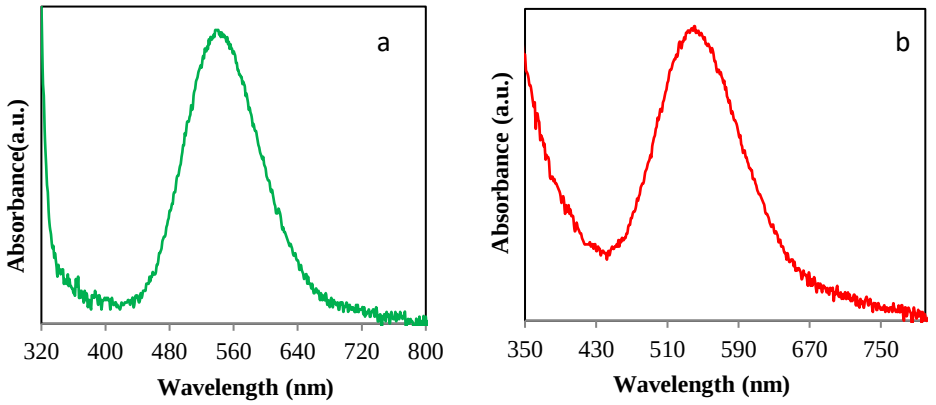

Figure 5: (a) UV-vis spectrum of $[Cu(Cm)(H_2O)_2](J)_2.2H_2O$ and (b) $[Cu(Cm)(S)_2](J)_2.2H_2O$.

The calculated magnetic moment (μ_{eff}) of $[Cu(Cm)(H_2O)_2](J)_2.2H_2O$ was 2.0 Bohr magnetons at 298 K. This value (1.80-2.26 B.M.) falls within the expected range for mononuclear patterned copper complex in the distorted octahedral shape geometry (Bain & Berry, 2008), suggesting that the complex likely adopts a similar structure. The agreement between the experimental μ_{eff} value and the theoretical range provides further evidence for the proposed coordination atmosphere of the copper(II) ion in the complex.

3.3. Synthesis and Structural Analysis of $[Cu(Cm)(S)_2](J)_2.2H_2O$

The reaction of $[Cu(Cm)(H_2O)_2](J)_2.2H_2O$ with the ligand S (4-hexadecyl pyridine) yielded the final complex $[Cu(Cm)(S)_2](L)_2$. $2H_2O$. This compound was isolated as a purple powder with 66.7 % yield. The elemental composition of the compound was determined to be Calc.: C, 63.4; H, 8.9; N, 6.7%. Found: C, 63.1; H, 8.5; N, 6.7%. These values closely matched (Table 1).

The FTIR analysis of $[Cu(Cm)(S)_2](L)_2.2H_2O$ exhibits characteristic peaks indicative of anticipated functional groups. A broad spectrum at 3440 cm^{-1} confirms the existence of O-H stretching vibrations associated with water molecules (Guo, Qing, Wu, & Wu, 2016). The N-H stretching vibration of pyridine part in the ligand L is observed at 3213 cm^{-1}. Additionally, peaks at 2851 and 2917cm^{-1} attributed to the symmetric and asymmetric C-H stretching modes of methylene groups, respectively (Mahmoudi *et al*., 2022). The C=N stretching frequency of the pyridine

moiety is evident at 1638 cm^{-1}, while the peaks of carboxylate group appear at 1472 and 1638 cm^{-1} correspond to symmetric and asymmetric C-O stretching vibrations, respectively. The frequency of stretching of the C-O ether part in the ligand is observed at 1192 cm^{-1}, and the C-N stretching frequency of the cyclam moiety is seen at 1192 cm^{-1} (Ahluwalia, 2023). The calculated ΔCOO value of 166 cm^{-1} suggests that the 4-ClC_6H_4COO- ions are not coordinated to the metal center, as reported in previous studies (Naima, 2016). The FTIR results are shown in the Figure 4.

The UV-vis spectrum of the complex $[Cu(Cm)(S)_2](J)_2.2H_2O$ displayed a broader d-d absorption band centered to the 542 nm (ε_{max} = 102.65 M^{-1} cm^{-1}), which is suggestive of a trans-III octahedral shape (Czekański *et al*., 2016). This spectral observation aligns with the previously characterized complex $[Cu(Cm)(H_2O)_2](J)_2.2H_2O$, suggesting that the copper(II) ion in the current complex is also surrounded by a similar octahedral arrangement of ligands (Christensen & Steele, 2023). The UV results are shown in the Figure 5b.

The magnetic moment (μ_{eff}) of the complex $[Cu(Cm)(S)_2](J)_2.2H_2O$ was calculated at 298 K which is 1.7 B.M., consistent with a mononuclear copper(II) complex in an octahedral shape geometry. However, it was lower than the μ_{eff} value of the ligand (S) free complex, $[Cu(Cm)(H_2O)_2](J)_2.2H_2O$ (1.9 BM), suggesting an influence of the ligand (S). The electron-releasing nature of the alkyl group in L strengthens the N-Cu(II) bonds in axial direction, leading to a less distortion in octahedral geometry and a slightly reduced μ_{eff} value.

Based on the instrumental data analysis and theoretical background the possible structure of the compound is illustrated in the Figure 6.

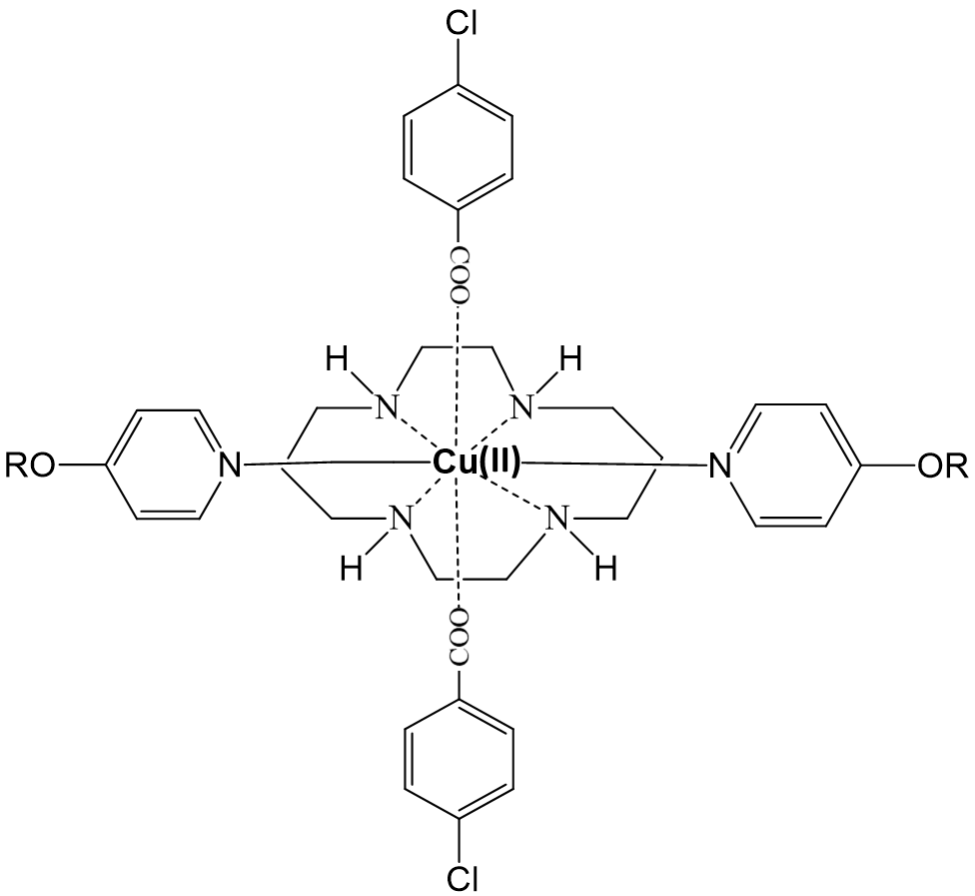

Figure 6: Tentative structure of $[Cu(Cm)(S)_2](J)_2.2H_2O$. (R = $OC_{16}H_{33}$); lattice H_2O are not shown for simplifying the diagram. Where Ligand (S); (4-$CH_3(CH_2)_{15}OC_5H_4N$); Cyclam (Cm); 1,4,8,11-Tetraazacyclotetradecane; J; 4-$ClC_6H_4COO^-$.

3.4. Thermal Behaviour of $[Cu(Cm)(H_2O)_2](J)_2.2H_2O$ and $[Cu(Cm)(S)_2](J)_2.2H_2O$

Thermogravimetric analysis (TGA) of $[Cu(Cm)(H_2O)_2](J)_2.2H_2O$ (Figure 7a) revealed a two-step weight loss profile. Lattice water molecules evaporated between 69 and 103 °C, causing a first weight reduction of 5.0% (expected: 5.6%). A subsequent major weight loss of 81.4% (expected: 84.6%) occurred between 240-660 °C, corresponding to the loss of coordinated water, decomposition of the cyclam ligand, and the 4-ClC_6H_4COO- anions. A residual mass of 13.6% (expected: 9.8% for CuO) remained at temperatures above 642 °C. These results align with the expected thermal decomposition pathway and demonstrate a significant thermal stability.

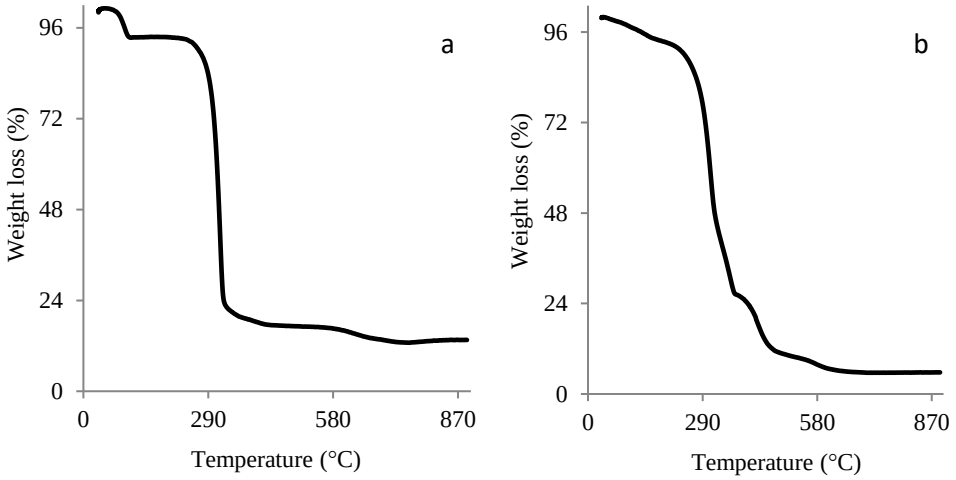

Figure 7: (a) TGA of $[Cu(Cm)(H_2O)_2](J)_2.2H_2O$ and (b) $[Cu(Cm)(S)_2](J)_2.2H_2O$.

TGA analysis of compound $[Cu(Cm)(S)_2](L)_2.2H_2O$ revealed a two-step weight loss profile (Figure 7b). An initial weight loss of 5.0% (expected: 5.5%) between 74 °C and 148 °C due to the loss of moisture. Afterward, a substantial weight loss of 89.0% (expected: 84.6%) arose between 225 °C and 674 °C, consistent to the disintegration of coordinately bound water, the macrcyclic ligand, 4-hexadecyloxypyridine ligands, and 4-ClC_6H_4COO- ions. A residual mass of 5.9% (expected: 9.8% assuming CuO) remained above 675 °C. These findings corroborate the proposed chemical formula of compound $[Cu(Cm)(S)_2](J)_2.2H_2O$. The observed decomposition temperature of 226 °C demonstrates thermal stability.

3.5. Mesomorphic Properties of the Complex $[Cu(Cm)(S)_2](J)_2.2H_2O$

Using polarized optical microscopy (POM) to understand optical textures and differential scanning calorimetry (DSC) to detect phase transitions, the mesomorphic behavior of the compound $[Cu(Cm)(S)_2](J)_2.2H_2O$ was examined. The findings are displayed in Figure 8.

Differential Scanning Calorimetry (DSC) analysis of final compound $[Cu(Cm)(S)_2](J)_2.2H_2O$ revealed a complex thermal behavior. Upon heating, three endothermic peaks were observed (Figure 8a). The first endotherm at 42.0 °C corresponds to a crystal-to-mesophase transition with $\Delta H = +35.6$ kJ mol^{-1}, while the second endotherm at 81.3 °C signifies a mesophase-to-mesophase transition with $\Delta H = +16.4$ kJ mol^{-1}. The conversion from the mesogenic phase to the uniform liquid phase is shown by the endothermic peak arose at 111.7 °C, where $\Delta H = +28.8$ kJ mol^{-1}. One exothermic peak has been observed during cooling (Figure 8b). The exothermic peak at 77.0 °C links to the uniform liquid-to-mesogenic phase conversion with $\Delta H = -26.5$ kJ mol^{-1}. These results suggested that the final compound exhibits mesophases and demonstrates a rich thermal behavior.

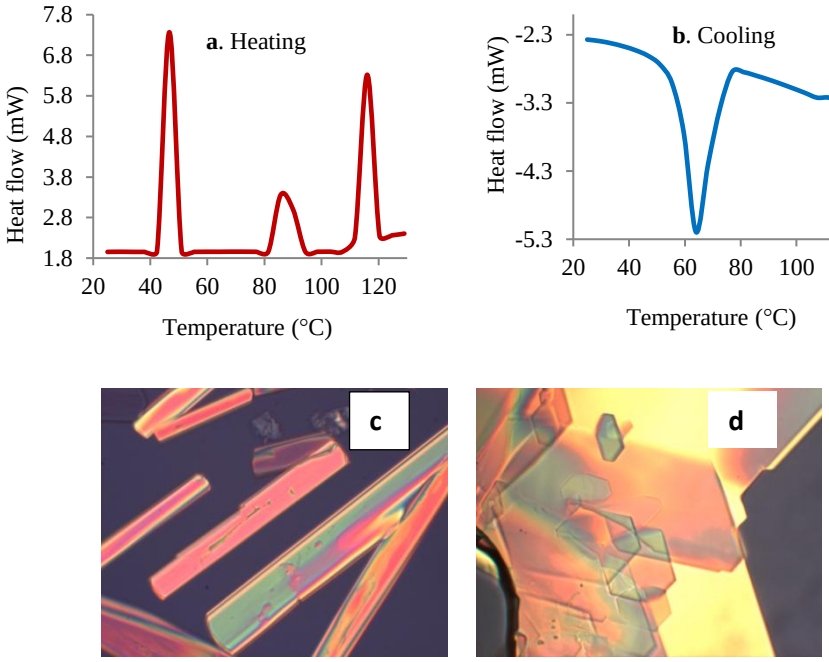

Figure 8: Mesogenic properties evaluation of $[Cu(Cm)(S)_2](J)_2.2H_2O$ by DSC and POM. DSC of (a) heating and (b) cooling in the temperature range of 29 to 129 °C. Photomicrographs (on cooling) of $[Cu(cyclam)(S)_2](J)_2.2H_2O$ at: (c) 100 °C and (d) 84 °C.

Compound $[Cu(Cm)(S)_2](J)_2.2H_2O$ exhibited metallomesogenic behavior, as evidenced by its thermal behavior and optical properties. The compound melted at 45.0 °C and changed into an isotropic liquid phase at 113.0 °C when examined using a polarized optical microscope (POM). The development of a distinctive optical pattern at 100 °C upon cooling suggested the existence of a mesophase (Figure 8c). The texture merged at 84 ºC (Figure 8d) on cooling more. This observation confirms the mesogenic nature of the final compound $[Cu(Cm)(S)_2](J)_2.2H_2O$, suggesting its potential for applications in liquid crystal displays and other optoelectronic devices.

4. Conclusion

In this study, a novel copper(II)-based metallomesogen, $Cu(Cm)(S)_2(J)_2 \cdot 2H_2O$, was successfully synthesized and characterized. The complex demonstrated a trans-III octahedral geometry around the copper center, confirmed through elemental analysis, UV-Vis spectroscopy, magnetic measurements, and thermal analysis. The compound exhibited mesomorphic behavior, with phase transitions observed through DSC and confirmed by polarized optical microscopy, highlighting its potential as a metal containing liquid crystal material. Furthermore, the magnetic susceptibility study indicated a mononuclear copper(II) system with slight distortion from ideal octahedral geometry. The unique combination of thermal stability,

mesophase formation, and magnetic properties positions this metallomesogen as a promising candidate for future applications in molecular electronics, display technologies, and smart materials. Future work could focus on tuning the mesomorphic and magnetic properties by modifying ligand structures or incorporating different metal centers, aiming to develop customized metallomesogens for specific technological applications.

Acknowledgement

The authors would like to express sincere gratitude to Assoc. Prof. Dr. Norbani Abdullah, from the Department of Chemistry, University of Malaya. This research was generously supported by the University of Malaya through research grants FP008/2011A, PV056/2012A, and UM.C/625/1/HIR/MOHE/CHAN/05. Furthermore, the authors would like to extend heartfelt thanks to all the dedicated staff members of the Department of Chemistry, University of Malaya.

Conflict of interest

The authors of this work have disclosed no conflicts of interest at any point.

References

Ahluwalia, V. (2023). Infrared Spectroscopy *Instrumental Methods of Chemical Analysis* (pp. 179-231): Springer.

Aljamali, N. M., & Molim, J. R. (2021). Review on engineering designs for laboratory chemical devices and displays. *Journal of Control and Instrumentation Engineering, 7*(2), 38-46.

Andrienko, D. (2018). Introduction to liquid crystals. *Journal of Molecular Liquids, 267*, 520-541.

Bain, G. A., & Berry, J. F. (2008). Diamagnetic corrections and Pascal's constants. *Journal of Chemical Education, 85*(4), 532.

Brandenburg, K., & Putz, H. (2006). Diamond. *Crystal Impact GbR, Bonn, Germany*.

Chakrabarty, S., Mim, R. M., Tonu, N. T., Ara, M. H., & Dhar, P. K. (2024). Removal of Toxic Pb (II) Ion from Aqueous Solution Using ZnO/K2SO4 Nanocomposites: Kinetics, Isotherms and Error Function Analyses. *Chemistry Africa, 7*(3), 1467-1480.

Chakrabarty, S., Tamim, A., Yılmaz, M., Dhar, P. K., Mim, R. M., & Dutta, S. K. (2023). Adsorption of Pb (II) ions from aqueous solution using CuO-ZnO nanocomposites. *Chemistry Africa, 6*(3), 1449-1462.

Cho, J., & Ishida, Y. (2017). Macroscopically oriented porous materials with periodic ordered structures: from zeolites and metal–organic frameworks to liquid-crystal-templated mesoporous materials. *Advanced Materials, 29*(25), 1605974.

Christensen, E. G., & Steele, R. P. (2023). Structural, Thermodynamic, and Spectroscopic Evolution in the Hydration of Copper (II) Ions, Cu2+ (H2O) 2− 8. *The Journal of Physical Chemistry A, 127*(32), 6660-6676.

Chukwu, J. E., & Lohdip, A. (2024). Spectroscopic Analyses of Alkaloids and Tannins from the Leaves of Ficus Citrifolia. *Path of Science, 10*(8), 4001-4008.

Cook, T. R., & Stang, P. J. (2015). Recent developments in the preparation and chemistry of metallacycles and metallacages via coordination. *Chemical reviews, 115*(15), 7001-7045.

Cuerva, C., Cano, M., & Lodeiro, C. (2021). Advanced functional luminescent metallomesogens: the key role of the metal center. *Chemical reviews, 121*(20), 12966-13010.

Czekański, Ł., Hoffmann, S. K., Barczyński, P., Gąsowska, A., Bregier-Jarzębowska, R., Zalewska, A., Katrusiak, A. (2016). Crystal structure and physical properties of 1-methyl-3-(carboxymethyl) benzimidazolium betaine· $CuBr_2$ in crystal and water solution. *New Journal of Chemistry, 40*(12), 10526-10535.

Dwivedi, N., Sunkari, S. S., Verma, A., & Saha, S. (2018). Molecular packing dependent solid state fluorescence response of supramolecular metal–organic frameworks: phenoxo-bridged trinuclear Zn (II) centered schiff base complexes with halides and pseudohalides. *Crystal Growth & Design, 18*(9), 5628-5637.

Forensi, S., Stopin, A., de Leo, F., Wouters, J., & Bonifazi, D. (2020). 1, 8, 10-Trisubstituted anthracenyl hydrocarbons: Towards versatile scaffolds for multiple-H-bonded recognition arrays. *Tetrahedron, 76*(51), 131299.

Ghosh, T. (2024). Synthesis, Thermotropic Properties, and Applications of Porphyrin-based Liquid Crystals: A Comprehensive Review. *Current Organic Chemistry, 28*(11), 857-889.

Guo, F., & Hurt, R. (2017). Supramolecular synthesis of graphenic mesogenic materials. *Chemical Synthesis and Applications of Graphene and Carbon Materials*, 69-85.

Guo, X., Qing, Y., Wu, Y., & Wu, Q. (2016). Molecular association of adsorbed water with lignocellulosic materials examined by micro-FTIR spectroscopy. *International Journal of Biological Macromolecules, 83*, 117-125.

Islam, M. H., Ara, M. H., Naime, J., & Khan, M. A. R. (2024). Nutritional evaluation of fish scale of selected saline and fresh water fish species. *Food and Humanity, 2*, 100225.

Islam, M. H., Hosna Ara, M., Khan, M. A., Naime, J., Khan, M. A. R., Rahman, M. L., & Ruhane, T. A. (2025). Preparation of Cellulose Nanocrystals Biofilm from Coconut Coir as an Alternative Source of Food Packaging Material. *ACS omega, 10*(9), 8960-8970.

Islam, M. H., Hosna Ara, M., Khan, M. A., Naime, J., Rahman, M. L., Ruhane, T. A., & Khan, M. A. R. (2024). A Sustainable Approach for the Development of Cellulose-Based Food Container from Coconut Coir. *ACS omega, 10*(1), 157-169.

Islam, M. J., & Islam, M. H. (2025a). Engineering Amphiphilic Gold Thiolate Clusters for Enhanced Luminescence and Controlled Assembly. *Chemical Physics Impact*, 100877.

Islam, M. J., & Islam, M. H. (2025b). Tuning emission and bandgap dynamics of $MAPbBr_3$ single crystals through halide exchange with methyl iodide. *Chemical Physics Impact, 10*, 100807.

Karpagakalyaani, G., Magdaline, J. D., & Chithambarathanu, T. (2022). Comparative spectral (FT-IR, FT-Raman, UV) investigations, HOMO–LUMO, NBO and in-silico docking analysis of Nikethamide, niazid and 2-Mercaptonicotinic acid. *Journal of Molecular Structure, 1252*, 132032.

Kawano, S.-i., Murai, T., Harada, T., & Tanaka, K. (2018). Columnar liquid-crystalline macrocycles synthesized via metal ion-assisted self-assembly. *Inorganic Chemistry, 57*(7), 3913-3919.

Kluenker, M., Mondeshki, M., Nawaz Tahir, M., & Tremel, W. (2018). Monitoring thiol–ligand exchange on Au nanoparticle surfaces. *Langmuir, 34*(4), 1700-1710.

Koifman, O. I., Ageeva, T. A., Beletskaya, I. P., Averin, A. D., Yakushev, A. A., Tomilova, L. G., Martynov, A. G. (2020). Macroheterocyclic compounds a key building block in new functional materials and molecular devices. *Macroheterocycles, 13*(4), 311-467.

Li, C., Li, Q., Kaneti, Y. V., Hou, D., Yamauchi, Y., & Mai, Y. (2020). Self-assembly of block copolymers towards mesoporous materials for energy storage and conversion systems. *Chemical Society Reviews, 49*(14), 4681-4736.

Li, Q., & Li, Z. (2020). Molecular packing: another key point for the performance of organic and polymeric optoelectronic materials. *Accounts of chemical research, 53*(4), 962-973.

Li, Z., & Yin, Y. (2019). Stimuli-responsive optical nanomaterials. *Advanced Materials, 31*(15), 1807061.

Liu, J., Zhang, Q.-h., Ma, F., Zhang, S.-f., Zhou, Q., & Huang, A.-m. (2020). Three-step identification of infrared spectra of similar tree species to Pterocarpus santalinus covered with beeswax. *Journal of Molecular Structure, 1218*, 128484.

Macrae, C. F., Edgington, P. R., McCabe, P., Pidcock, E., Shields, G. P., Taylor, R., Streek, J. (2006). Mercury: visualization and analysis of crystal structures. *Applied Crystallography, 39*(3), 453-457.

Mahmoudi, G., Sahli, S., Tamer, Ö., Çınar, E. B., Böhme, U., Dege, N., Kaabi, K. (2022). Investigation on crystal structure, spectral FT-IR analysis, DFT and molecular docking studies of a novel complex with the N′-(pyridin-2-ylmethylene) nicotinohydrazide. *Journal of Molecular Structure, 1269*, 133741.

Marti-Centelles, V., Pandey, M. D., Burguete, M. I., & Luis, S. V. (2015). Macrocyclization reactions: The importance of conformational, configurational, and template-induced preorganization. *Chemical reviews, 115*(16), 8736-8834.

Naima, S. (2016). *Magnetic metallomesogenic complexes of Cu (ii), Ni (ii), Co (ii), and Mn (ii) with cyclam and substituted arylcarboxylates/Naima Sharmin.* University of Malaya.

Nasiri Sovari, S., & Zobi, F. (2020). Recent studies on the antimicrobial activity of transition metal complexes of groups 6–12. *Chemistry, 2*(2), 418-452.

Rosenthal, E. Q., Puskas, J. E., & Wesdemiotis, C. (2012). Green polymer chemistry: Living dithiol polymerization via cyclic intermediates. *Biomacromolecules, 13*(1), 154-164.

Santos, A. F., Figueirinhas, J. L., Dionísio, M., Godinho, M. H., & Branco, L. C. (2024). Ionic Liquid Crystals as Chromogenic Materials. *Materials, 17*(18), 4563.

Sharmin, N., Islam, M. J., Islam, M. H., Refat, M. S., Mohsen, Q., & Alsuhaibani, A. M. (2025). Mesomorphic and themochmical behavior of a Cu (II)-cyclam ionic liquid: A novel approach to metallomesogens. *Bulletin of the Chemical Society of Ethiopia, 39*(7), 1381-1394.

Sheldrick, G. M. (2008). A short history of SHELX. *Foundations of crystallography, 64*(1), 112-122.

Thakur, M. S., Singh, N., Sharma, A., Rana, R., Syukor, A. A., Naushad, M., . . . Singh, L. (2022). Metal coordinated macrocyclic complexes in different chemical transformations. *Coordination Chemistry Reviews, 471*, 214739.

Wang, Y., Astruc, D., & Abd-El-Aziz, A. S. (2019). Metallopolymers for advanced sustainable applications. *Chemical Society Reviews, 48*(2), 558-636.

Wang, Z., Dan, G., Zhang, R., Ma, L., & Lin, K. (2023). Coupling and decoupling CH stretching vibration of methylene and methine in serine conformers. *Spectrochimica Acta Part A: Molecular and Biomolecular Spectroscopy, 285*, 121829.

Xu, D., Li, Y., Yin, S., & Huang, F. (2024). Strategies to address key challenges of metallacycle/metallacage-based supramolecular coordination complexes in biomedical applications. *Chemical Society Reviews*.

Yin, K., Hsiang, E.-L., Zou, J., Li, Y., Yang, Z., Yang, Q., Wu, S.-T. (2022). Advanced liquid crystal devices for augmented reality and virtual reality displays: principles and applications. *Light: Science & Applications, 11*(1), 161.

Yufanyi, D. M., Abbo, H. S., Titinchi, S. J., & Neville, T. (2020). Platinum (II) and Ruthenium (II) complexes in medicine: Antimycobacterial and Anti-HIV activities. *Coordination Chemistry Reviews, 414*, 213285.

Yusuf, M. O. (2023). Bond characterization in cementitious material binders using Fourier-transform infrared spectroscopy. *Applied Sciences, 13*(5), 3353.